Arts & Sciences Articles

Arts and Sciences

10-16-2017

Integration of swimming kinematics and ram suspension feeding in a model American paddlefish, Polyodon spathula

Grant Emerson Haines
William & Mary, gehaines@email.wm.edu

S. Laurie Sanderson
College of William and Mary, slsand@wm.edu

RESEARCH ARTICLE

Integration of swimming kinematics and ram suspension feeding in a model American paddlefish, *Polyodon spathula*

Grant E. Haines*,‡ and S. Laurie Sanderson

ABSTRACT

Ram suspension-feeding fishes swim with an open mouth to force water through the oral cavity and extract prey items that are too small to be pursued individually. Recent research has indicated that, rather than using a dead-end mechanical sieve, American paddlefish (*Polyodon spathula*) employ vortical cross-step filtration. In this filtration mechanism, vortical flow that is generated posterior to the branchial arches organizes crossflow filtration processes into a spatial structure across the gill rakers. Despite the known impact of locomotor kinematics on fluid flow around the bodies of swimming fish, the effects of locomotor kinematics on filtration mechanisms in ram suspension feeders are unknown. Potential temporal organization of filtration mechanisms in ram suspension-feeding fish has not been studied previously. We investigated the effects of locomotor kinematics associated with undulatory swimming on intra-oral flow patterns and food particle transport. A mechanized model of the oral cavity was used to simulate the swimming kinematics of suspension-feeding paddlefish. We recorded fluctuations of flow speed and pressure within the model, which occurred at a frequency that corresponded with the frequency of the model's strides. Using the mechanized model in a flow tank seeded with *Artemia* cysts, we also showed that swimming kinematics aided the transport of this simulated food to the posterior margins of the gill slots, although the time scale of this transport is expected to vary with prey parameters such as size and concentration. Dye stream experiments revealed that, although stable vortical flow formed because of flow separation downstream of backward-facing steps in control trials, vortical flow structures in mechanized trials repeatedly formed and shed. These findings suggest strong integration between locomotor and feeding systems in ram suspension-feeding fishes.

KEY WORDS: Crossflow filtration, Backward-facing steps, Filter-feeding fish, Gill rakers, Branchial arches, Yaw

INTRODUCTION

Suspension-feeding fish, which feed on prey items that are too small to be efficiently pursued and captured individually, are both ecologically (Zamon, 2003; Tanaka et al., 2006) and economically important (Food and Agriculture Organization of the United Nations, 2016). These fish may engulf their prey by oral pumping, which generates a suction that is used to force water

Department of Biology, College of William & Mary, Williamsburg, VA 23187-8795, USA.
*Present address: Department of Biology, McGill University, Montréal, Québec, Canada H3A 0C4.

‡Author for correspondence (grant.haines@mail.mcgill.ca)

G.E.H., 0000-0001-9085-0022; S.L.S., 0000-0002-5717-1981

through the oral cavity, allowing water currents and filter structures to separate prey from the water. Alternatively, suspension-feeding fish may force water through their oral cavities by opening their mouths and swimming forward, or 'ramming'. Ram feeding and suction feeding are not discrete classifications, but describe two ends of a spectrum (Norton and Brainerd, 1993). However, the morphologies and feeding behavior of ram suspension-feeding fish are more extreme than those of other ram feeders, and their oral anatomies are distinctly adapted for the capture of very small prey. In addition to an unusually large gape (Ferry et al., 2015), these adaptations may include filter pads, as in whale sharks and mobulid rays (Paig-Tran and Summers, 2014), or thin bony or cartilaginous structures attached to the branchial arches called gill rakers, as in the paddlefish (Rosen and Hales, 1981), basking shark (Paig-Tran and Summers, 2014) and teleost suspension feeders (Friedland et al., 2006; Sanderson et al., 1996; Castillo-Rivera et al., 1996).

Until recently, the gill rakers of most suspension-feeding fish were assumed to function as a dead-end sieve, in which water flowed between the rakers and food particles larger than the inter-raker space were retained, as in bream (Hoogenboezem et al., 1993; Hoogenboezem, 2000). Additional mechanisms for the capture of particles include inertial impaction and direct interception by filter structures (Rubenstein and Koehl, 1977; LaBarbera, 1984; Shimeta and Jumars, 1991), often with the aid of mucus (Sanderson et al., 1991). The sieve filtration model that had been assumed to describe filtration in all taxa of suspension-feeding fishes has been replaced for many species by a crossflow filtration model. In crossflow filtration, particle-laden water flows across the surface of a filter, rather than perpendicular to the filter. Particles in crossflow remain in suspension and are transported posteriorly as water is forced out of the oral cavity through the rakers (Sanderson et al., 2001; Brainerd, 2001). Importantly, crossflow filtration mechanisms allow the capture of particles smaller than the spaces between filter structures, and reduce fouling of the filter (Brainerd, 2001; Callan and Sanderson, 2003; Cheer et al., 2012).

Crossflow alone does not appear to be entirely responsible for the lack of filter fouling in suspension-feeding fish (Sanderson et al., 2001; Brainerd, 2001). Elaborations of the fish crossflow model have been developed recently to address the flow separation that occurs posterior to the branchial arches and how the resulting vortical flow changes the spatial structure of filtration mechanisms in ram suspension feeders with rib-and-groove branchial arch and gill raker arrangements, specifically the American paddlefish and the basking shark (Sanderson et al., 2016). In stationary physical models of these species, the branchial arches form backward-facing steps that generate persistent vortical flow structures along the gill raker surfaces (Sanderson et al., 2016). However, no research to date has shown how continuous motion related to swimming kinematics influences intra-oral flow patterns or reduces filter fouling during ram suspension feeding.

The most common modes of swimming in fish require the passage of an undulatory wave along the length of an individual's body, providing thrust and allowing the fish to propel itself forward through the water (Webb, 1975). The characteristics of these waves, as well as the size and morphology of the fish to which they belong, determine a fish's swimming speed and how quickly it can accelerate (Tytell et al., 2010; Webb et al., 1984). Even in the undulatory swimmers with very low amplitude undulatory waves, as in tuna, there is some yaw (lateral rotation of the head about a vertical axis as a consequence of undulatory wave production), and there is no point on the body of the fish where the amplitude of the propulsive wave is zero (Dewar and Graham, 1994; Webb, 1992). As a result of the wave having a nonzero amplitude across the entire length of the fish, heave (defined as linear motion perpendicular to the swimming direction, effectively half the amplitude of an undulatory wave at a given point; Akanyeti et al., 2016; Shelton et al., 2014; Müller et al., 2002) is an important measurement used to describe the wave at a particular point on the body. Amplitude, and therefore heave, must increase towards the caudal end to provide a propulsive force (Webb, 1975; Shelton et al., 2014; Weihs, 2002). There is a phase difference between yaw angle and heave, and this phase difference may have important functional implications (Lighthill, 1993; Rowe et al., 1993; Akanyeti et al., 2016). For instance, locomotor kinematics including yaw, heave and the phase difference between them have been shown experimentally (Akanyeti et al., 2016) and theoretically (Lighthill, 1993) to improve lateral line sensing by the reduction of self-generated pressure noise. Akanyeti et al. (2016) have also demonstrated that locomotor regulation of pressures surrounding the head is likely used by fish to reduce the energetic cost of opercular pumping for respiration. However, the possible effect of locomotor kinematics on intra-oral flow speed and pressure dynamics during ram suspension feeding have not yet been explored.

Kane and Higham (2015) suggested that by taking an integrative approach to the study of different biological processes, we can better understand how these processes interact to influence performance and fitness outcomes. To the extent that processes interact, variation in one process may influence performance of the other, ultimately resulting in variable fitness outcomes and at population scales potentially influencing evolution (Kane and Higham, 2015; Higham et al., 2016). Although Kane and Higham (2015) used locomotor and feeding systems of fish to demonstrate the benefits of an integrated approach to biomechanics, they suggested that ram suspension-feeding fish exhibit only weak integration between these systems.

We demonstrate here, using an American paddlefish [*Polyodon spathula* (Walbaum 1792)] model, that the kinematics of undulatory locomotion and the function of branchial arches and gill rakers as filtration structures are in fact strongly integrated, both in space and in time. We conducted experiments showing that in a 3-D printed model, the yaw and heave that we quantified in live suspension-feeding paddlefish caused fluctuations in intra-oral pressures and flow speeds. We also visualized these flow patterns generated by locomotor kinematics using dye streams, and used *Artemia* cysts to show the influence of cyclical flow patterns on food particle capture and transport in a 3-D model of a ram suspension-feeding paddlefish.

MATERIALS AND METHODS
Physical model
To simulate the oral cavity of a paddlefish, we designed a 3-D model using SketchUp Make software (version 16.1.1451,

Trimble, Sunnyvale, CA, USA), and printed of nylon plastic (fine polyamide PA 2200) by Shapeways Inc. (New York, NY, USA) (Fig. 1). The model's branchial arch angles were derived from measurements of three paddlefish specimens [32.5–45.5 cm total length (TL); 18–29 cm eye–fork length (EFL)] preserved in as close as possible to ram suspension-feeding position. These three plus an additional fourth specimen (39 cm TL, 22 cm EFL), all obtained on ice from aquaculture facilities within 24 h of death (William and Mary Institutional Animal Care and Use Committee approval 07/30/14; Virginia Department of Inland Fisheries Approval 07/24/14), were used to confirm that the proportions of the model were realistic and to estimate the TL and EFL of a paddlefish with an oral cavity the size of the model (36.9 cm TL, 21.1 cm EFL; Table 1).

The model's three anterior arches extended from the ventral midline to the dorsal midline, and the fourth branchial arches extended only over the ventral portion of the model (Burggren and Bemis, 1992). To simulate gill rakers, the model's gill slots were covered with a nylon mesh (pore diameter 140 µm, thread diameter 50 µm, 55% open pore area; Component Supply Co., Fort Meade, FL, USA). No mesh fabric can perfectly simulate the rakers of a paddlefish, which run parallel to each other rather than
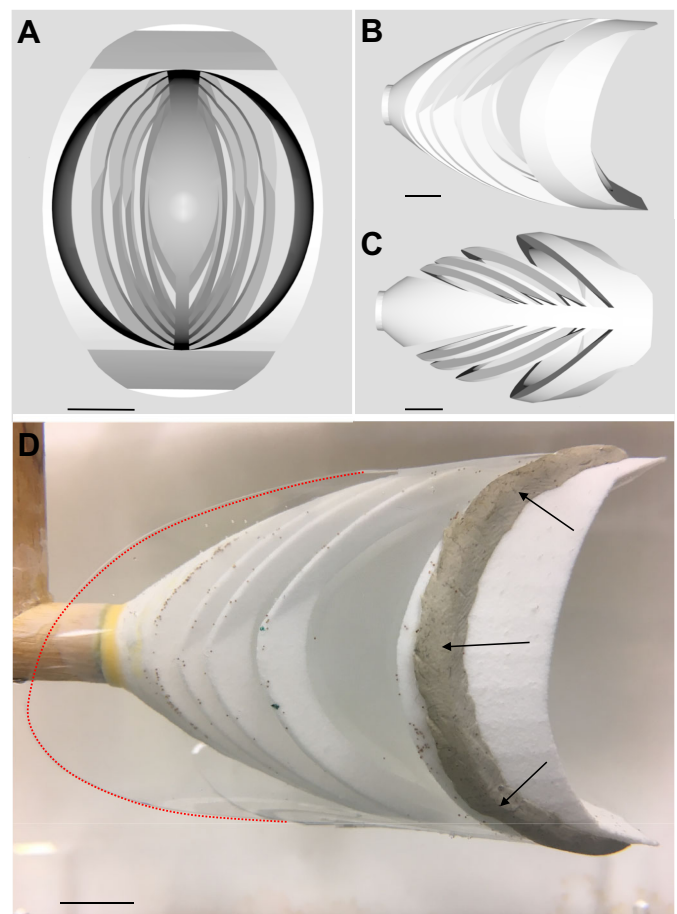
Fig. 1. The 3-D printed model and experimental setup. (A–C) A digital rendering of the 3-D printed model that we designed for all experiments, shown from anterior (A), lateral (B) and dorsal (C) views. (D) A photograph of the model set up in the recirculating flow tank. In D, the dashed red line indicates the posterior extent of the vinyl operculum, and the arrows indicate where the anterior edge of the operculum is affixed to the model beneath the caulk. The model is 52 mm tall and 74 mm long. Scale bars, 1 cm.

Table 1. Morphometric measurements (cm) of preserved paddlefish specimens and analogous measurements of the 3-D printed model

	Fish						
	1	2	3	4	Mean	s.d.	Model
TL	32.5	35.5	45.5	39.0	38.13	5.59	36.92*
EFL	18.0	19.0	29.0	22.0	22.0	5.0	21.1‡
Esophagus–anterior maxilla	4.8	6.0	8.5	6.3	6.4	1.54	6.84
Third branchial arch–anterior maxilla	4.3	5.2	7.1	5.5	5.53	1.17	5.44
Gape width	3.8	4.5	5.4	4.2	4.48	0.68	4.24
Gape height	3.4	3.2	2.0	2.1	2.68	0.73	4.18
TL ratio (X/TL)							
EFL	0.55	0.54	0.64	0.56	0.573	0.045	
Esophagus–anterior maxilla	0.15	0.17	0.19	0.16	0.166	0.016	
Third branchial arch–anterior maxilla	0.13	0.15	0.16	0.14	0.144	0.001	
Gape width	0.12	0.13	0.12	0.11	0.118	0.008	
Gape height	0.10	0.09	0.04	0.05	0.073	0.029	

For measurements to 'anterior maxilla', the most anterior point on the midline of the maxilla was used. For third branchial arch–anterior maxilla measurements, the anterior edge of the most posterior portion of the bend in the arch was used. A larger gape height was used in the model to facilitate mesh application and viewing during trials. Although it fell outside of the range of measurements from preserved specimens, the gape height used was within an anatomically plausible range for a live suspension-feeding paddlefish.

*The estimated total length (TL) for the model is a mean of the TLs calculated using the four specimens' mean third branchial arch–anterior maxilla/TL and gape width/TL ratios.

‡The estimated eye–fork length (EFL) was calculated using the TL, obtained as described above, and the specimens' mean EFL/TL ratio.

crossing each other like the fabric of the mesh. However, the mesh used in our model approximately simulates the inter-raker distance and the thickness of the rakers themselves (42 and 100 µm, respectively, for a paddlefish of 21 cm EFL; Table 1) (Rosen and Hales, 1981). Rather than cut the threads of the mesh running vertically, leaving only the threads in the anterior–posterior direction to simulate the gill rakers, we left the threads of the mesh running in both directions intact. This was necessary because the mesh threads are more flexible than the dermal bone gill rakers of paddlefish, and thus required support from the threads running vertically in order to maintain their position while in the flow tank. To cover the model's rounded shape, some stretching of the mesh was required. Using Loctite® Super Glue Gel Control™, the mesh was affixed to the model at the lateral edge of each branchial arch, as well as the anterior and posterior external surfaces of the edges of the first and last gill slots, respectively. A clear, flexible vinyl sheet (20 gauge) was attached with Loctite® Super Glue Gel Control™ and a thin band of Mortite™ caulking cord to the exterior of the model immediately posterior to the oral gape to simulate an operculum by covering all the model's gill slots (Fig. 1).

The aspect ratio of the model's first two gill slots (groove aspect ratio; Sanderson et al., 2016) was calculated using the distance between the medial edges of the slots on the central coronal plane as slot width. The lengths of the line segments extending perpendicularly from the lines used to measure slot width to the posterior lateral edge of each slot's anterior branchial arch were used for slot height. The aspect ratios were calculated to be 3.38 and 1.76 for the model's first and second gill slots, respectively.

This model was attached by a 0.95 cm diameter wooden dowel to a servo motor (RadioShack standard servo 2730766, 4.8–6 V), which controlled yaw, and to a DC motor on a repurposed printer printhead, belt and stabilizer bar, which controlled lateral heave. Arduino Uno and Arduino MotorShield hardware coordinated these motors using a program we designed with Arduino Genuino software (version 1.6.8; https://www.arduino.cc/en/Main/OldSoftwareReleases#previous), allowing the control of yaw and heave. We were also able to control the phase difference between yaw and heave, which Akanyeti et al. (2016) have noted is an important, but often ignored, kinematic variable in undulatory swimmers.

Analysis of live paddlefish swimming kinematics

Kinematic variables were measured using video (Panasonic WV-2170 video camera, 30 frames s^{-1}) recorded of live paddlefish (36–45 cm TL, 22–29 cm EFL) ram suspension feeding on adult brine shrimp in a round tank (1.2 m diameter×0.2 m deep; Sanderson et al., 1994). The camera was placed directly over the center of the tank (Sanderson et al., 1994). Kinematic variables were measured in nine video clips (mean±s.d. duration=2.7±1.4 s), in which the fish in the tank swam in a reasonably straight line without colliding with any structures or other fish in the tank while ram suspension feeding during at least a portion of each clip. Yaw and heave measurements (see Fig. 2) were taken from three separate fish, each of which appeared in three of the selected video clips.

Yaw

The experimental design allowed the paddlefish to ram suspension feed at a voluntary swimming speed, rather than requiring the fish to conform to a designated flume speed. However, the use of a circular tank necessitated that the yaw angle be corrected for the potential effects of a circular trajectory while swimming in the tank. For each frame of video in a given clip, we measured the rostrum angle as the angle of the midline of the fish's rostrum relative to a horizontal line on the video, using the protractor tool in ImageJ 1.49 (National Institutes of Health, Bethesda, MD, USA). A linear trend line was obtained in Microsoft Excel 15.30 representing the change in these measured rostrum angles over the duration of the clip.

The difference between the measured rostrum angle and the trend line at the corresponding time point was recorded as the yaw. The two points used as yaw maxima in each stride had the largest and smallest differences between the measured rostrum angle and the trend line. The absolute value of the difference between consecutive yaw maxima was divided by two, providing a mean maximum yaw angle for each stride (two tailbeats). These mean maximum yaw angles per stride were then averaged for each clip. This procedure corrected for the circular trajectory of the fish while swimming voluntarily in the tank. The mean maximum yaw angle and standard deviation for each fish and the overall mean maximum yaw angle and standard deviation for all three fish were weighted by the number of measurements per clip.

A
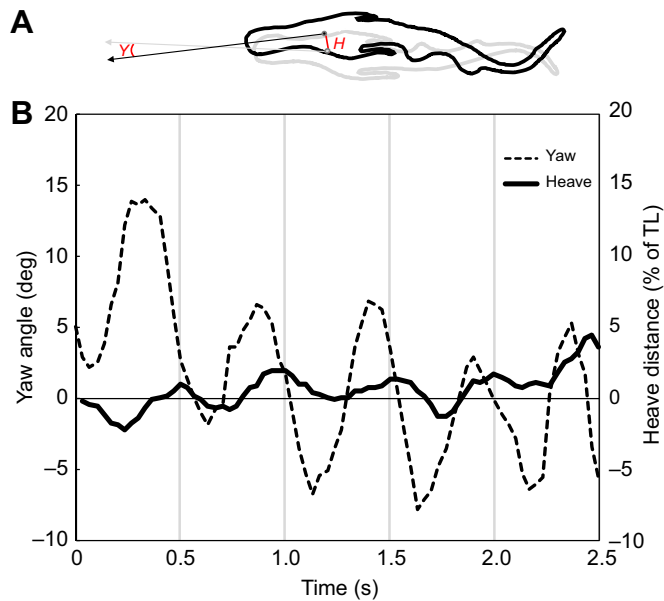
Fig. 2. Yaw and heave in the paddlefish. (A) Line drawings of a paddlefish in dorsal view at two times during its stride. The points represent the anterior edge of the oral cavity and the lines represent the midline of the rostrum. Yaw (*Y*) is shown as the difference in angle between the two rostrum midlines, and heave (*H*) is shown as the distance the point moved laterally between these times in the fish's stride. (B) Representative data showing the temporal relationship between yaw and heave over approximately five strides. Yaw is shown in degrees, and heave is shown as a percentage of the fish's total length (TL). For both variables, deviation from zero represents deviation from the trajectory of the fish over the duration of the video clip from which these calculations were made. For explanations of the specific points that were identified on each video frame and the methods for calculation of yaw and heave, see Materials and methods.

Stride length and swimming speed

Absolute measurements of the lengths of individual fish in the videos used to calculate swimming kinematics were unavailable. Therefore, measurements of speed of the swimming fish and stride length (the forward distance traveled during one complete undulatory wave) were taken in pixels and then converted into body lengths (TL) by dividing by the fish's TL (in pixels). Total length was measured from the anterior tip of the rostrum, down the midline of the fish to just below the posterior tip of the tail, as in Grande and Bemis (1991). To minimize the effect of yaw on these calculations, only the frames of video from which yaw maxima were measured were used, so stride length and swimming speed were measured per stride. This resulted in calculations for two sets of strides: one including frames with yaw maxima to the left, and one including frames with yaw maxima to the right.

To calculate stride length in ImageJ, we measured the linear distance in pixels traveled by the tip of the rostrum between the frames of video showing the yaw maxima. We then divided each stride length by the time elapsed between frames to calculate speed (pixels s^{-1}). We calculated the average speed and stride length over each series (yaw maxima to the left, and to the right) using the harmonic mean of speeds and stride lengths calculated for each stride, and then by finding the mean of both stride series from each clip. Harmonic means of speeds were weighted by the duration of each stride. Unweighted standard errors of harmonic means were calculated for each clip.

Heave and phase difference

During feeding, the oral cavity of paddlefish expands laterally as well as vertically, and the anterior edge of the oral cavity is located directly ventral to the eyes. Therefore, in each frame of video from the nine clips used to measure yaw, we were able to place a single point on the dorsal midline of the fish at the anterior edge of the oral cavity. The locations of these markings were tracked between frames using the Cartesian coordinates of their pixels in ImageJ, and the Euclidean distance was calculated between each pair of consecutive points. The distance traveled on the *x*-axis and the distance traveled on the *y*-axis between each pair of consecutive frames were both divided by the Euclidean distance traveled between frames, each yielding a number between −1 and 1. This process was repeated for all pairs of consecutive frames in each clip, and yielded one series of numbers between −1 and 1 for each axis. In Excel, we fit polynomial trend lines to both series that resulted from these calculations (one for the *x*-axis and one for the *y*-axis). Taking the difference between each trend line and the corresponding value between −1 and 1, and multiplying it by the total Euclidian distance traveled between frames yielded a deviation distance from the trajectory for each pair of consecutive frames.

From the deviations calculated along the *x*- and *y*-axes, we used the Pythagorean theorem to determine deviation from the fish's trajectory in two dimensions. We added these deviations from all consecutive frame pairs in a video clip to calculate cumulative heave distances for each frame pair. In each stride, heave maxima to both sides of the fish were identified, and the heave to either side was found by dividing the difference between consecutive heave maxima by two. All heave distances were converted into body lengths from pixels by dividing by the TL of the fish (in pixels).

Phase difference between yaw and heave was calculated by first identifying a yaw maximum, then determining the time elapsed between the yaw maximum and the associated heave maximum. The time elapsed between the first yaw maximum and the heave maximum was then divided by time elapsed between the first yaw maximum and the subsequent yaw maximum to the same side, yielding the phase difference between yaw and heave as a proportion of that stride. Mean phase difference throughout a video clip was calculated using all phase differences from yaw and heave maxima to both sides of the fish.

Application of live paddlefish kinematics to the model

All fish and total means from the video clips were weighted by the number of measurements per clip (Table 2). All fish standard deviations were calculated from clip means, weighted by the number of measurements per clip. Mean (±s.d.) yaw maximum was 6.07±2.13 deg (82 total measurements). The mean (±s.d.) measured heave maximum was 0.013±0.004 TL (74 total measurements). The mean (±s.d.) phase difference between yaw and heave cycles was 0.15±0.22 yaw cycles (53±77 deg, 73 total measurements). Mean stride length, stride period and speed were 0.36 TL, 0.48±0.09 s and 0.75 TL s^{-1}, respectively (72 measurements each). The mean stride frequency (the reciprocal of the mean stride period) was 2.1 Hz. The mean speed of 0.75 TL s^{-1} is equivalent to 27.8 cm s^{-1} for our model of a 36.9 cm TL paddlefish. Although comparable measurements were not always available for all these variables in the literature, most available measurements were similar to or larger than those that we recorded (Webb, 1986; Akanyeti et al., 2016; Müller et al., 2002; Webb, 1988, 1975). The exception was the phase difference between yaw and heave, which we measured to be larger at this swimming speed than Akanyeti et al. (2016), possibly

Table 2. Kinematic measurements of live, suspension-feeding paddlefish

Fish	Yaw (deg)	s.d.	n	Stride length (TL)	s.e.m.	Stride period (s)	s.d.	Speed (TL s⁻¹)	s.e.m.	n	Phase difference	s.d.	n	Heave (TL)	s.d.	n
1	5.62	2.38	5	0.490	0.040	0.883	0.196	0.557	0.044	4	0.091	0.264	4	0.017	0.008	3
	4.70	0.83	8	0.259	0.018	0.414	0.042	0.626	0.037	7	0.170	0.099	8	0.008	0.003	9
	5.04	2.90	8	0.253	0.026	0.469	0.143	0.564	0.035	7	−0.211	0.560	7	0.009	0.002	8
	5.05	**1.98**	**21**	**0.308**		**0.539**	**0.116**	**0.586**		**18**	**0.013**	**0.335**	**19**	**0.010**	**0.003**	**20**
2	7.14	3.23	8	0.411	0.024	0.495	0.085	0.835	0.027	6	0.219	0.099	8	0.015	0.006	10
	7.40	1.77	4	0.484	0.023	0.645	0.035	0.777	0.022	3	0.246	0.177	4	0.016	0.004	4
	7.65	1.46	5	0.554	0.034	0.560	0.061	0.997	0.013	4	0.192	0.137	5	0.013	0.004	5
	7.35	**2.44**	**17**	**0.472**		**0.550**	**0.063**	**0.872**		**13**	**0.217**	**0.117**	**17**	**0.015**	**0.005**	**19**
3	5.48	2.90	11	0.326	0.020	0.434	0.101	0.760	0.034	10	0.251	0.305	8	0.014	0.004	7
	6.15	1.61	27	0.347	0.007	0.427	0.076	0.805	0.021	26	0.187	0.100	23	0.013	0.005	21
	6.77	2.93	6	0.342	0.044	0.460	0.127	0.771	0.041	5	0.069	0.191	6	0.013	0.003	7
	6.07	**2.08**	**44**	**0.341**		**0.432**	**0.085**	**0.790**		**41**	**0.182**	**0.165**	**37**	**0.013**	**0.004**	**35**
Total	6.07	2.13	82	0.356		0.480	0.090	0.754		72	0.146	0.215	73	0.013	0.004	74

Stride length, stride period and speed were obtained using the same time points, so these calculations used the same number of measurements in each video clip. Measurements for each of three clips are shown in the first three rows for each fish. Phase difference is presented as the lag of a heave maximum in relation to the maximum of the concurrent yaw cycle. The value shown is a proportion of a yaw cycle, so that a value of 0.250 indicates that heave maxima occurred 25% of a yaw wave after yaw maxima. A negative value for this calculation indicates that the heave maxima preceded the yaw maxima. The final row for each fish includes totals for that fish. All grand totals and totals for individual fish are weighted by the number of measurements per clip or per fish, and all s.d. totals were calculated from pooled variances weighted by number of measurements per clip or per fish. Harmonic means were calculated for stride length. Harmonic means weighted by stride period were calculated for speed. Arithmetic means are shown for all other measurements. Standard errors were calculated only for harmonic means, and are unweighted.

owing, at least in part, to the influence of the paddlefish's long rostrum on its swimming.

Because of the small scale of the measured heave maxima in live fish, it was not possible to heave the model at these distances. In a test of the model, the mean heave distance to either side measured over four strides at a point approximately 7 mm posterior to the anterior dorsal edge of the model was 1.10±0.01 cm (±s.d.; n=8, two heave measurements per stride over four strides). In videos of live paddlefish, the mean heave measured was 0.013±0.004 TL, equivalent to 0.465±0.153 cm for a fish of the size simulated by our model (36.92 cm TL). However, analogous measurements made at the nose of subcarangiform fish have found undulatory wave amplitudes ranging from 0.04 to 0.07 TL, equivalent to heaves ranging from 0.02 to 0.035 TL (0.74–1.29 cm in a 36.92 cm fish), which show much greater agreement with our model (Webb, 1975; Bainbridge, 1958, 1963; Pyatetskiy, 1970a,b in Webb, 1975, 1971).

Operation of the models

All stationary control trials were conducted with the model positioned parallel to flow in the cross-sectional center of a recirculating flow tank (18×18×90 cm working area, 100 liters total volume). Based on our kinematic measurements of suspension-feeding paddlefish, mechanized trials in all experiments were conducted using a yaw of 5 deg to either side of the direction of flow, a heave of 1.1 cm, a phase difference of 72 deg (20% of one undulatory wavelength, i.e. 20% of one stride) between yaw and heave, and a stride frequency (corresponding with tail beat frequency in kinematic studies of live fish) of 2.2 Hz. Average flow velocity in the recirculating flow tank during experimental trials was 28.3 cm s⁻¹ (s.d.=0.4 cm s⁻¹, range 27.6–28.9 cm s⁻¹). The flow speed was measured using a Geopacks MFP51 flowmeter impeller (Hatherleigh, Devon, UK) positioned in the center of the flow tank, when the model was absent from the flow tank.

Particle transport

Experiments including both mechanized and stationary control trials were conducted to examine the effects of swimming kinematics on particle transport. All trials began 10 s after the flow tank was seeded with 1.20 g of brine shrimp cysts (*Artemia*, 210–300 μm diameter, density 1.09 g cm⁻³, 20 ppm volume concentration), and were recorded for 3 min (240 frames s⁻¹).

A rectangular area was demarcated on the exterior of the model, including the entire anterior to posterior width of the first four gill slots, and excluding the fifth gill slot. Mesh coverage by particles was analyzed in ImageJ using color thresholding and the 'Analyze Particles' tool on still frames taken from the video at 5 s intervals. Regions of mesh that were not covered by particles, but were nevertheless highlighted by the thresholding process, were manually reassigned as being clear of particles. Because the light
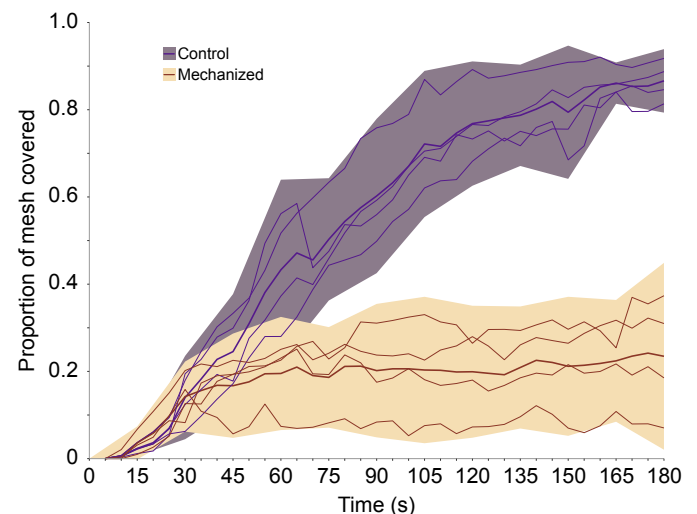
Fig. 3. Proportion of analyzed area of mesh covered by *Artemia* cysts during 3 min trials. Thick brown and purple lines represent the means of mechanized and control treatments, respectively. Coverage for trials in each treatment is shown at 5 s intervals throughout trials. Shaded regions represent 95% confidence intervals of the mean measured mesh coverage for trials at 15 s intervals within each treatment. The effects of treatment, time and treatment×time were significant (all P<0.0005, two-way repeated measures ANOVA, n=4 trials per group, 36 time points per trial).

conditions changed slightly as particles were captured in the model, video color and ImageJ threshold settings were changed in some trials to compensate. Care was taken in the analysis of mechanized trials to use frames of video that captured the model at an angle as close to parallel with respect to flow as possible. Frames analyzed for the mechanized model were sampled from no more than 0.45 s after each 5 s interval, except in the case of the final time point, when frames were used from the final stride of each mechanized trial. Proportion of mesh area covered within the demarcated region was calculated in each of these still frames. Areas of mesh covering exterior surfaces of branchial arches were excluded from these calculations. We used SPSS (IBM SPSS Statistics, Version 24, Armonk, NY, USA) to conduct Levene's test for homogeneity of variance and a two-way repeated-measures ANOVA to compare particle coverage of the mesh throughout the trials. For the purpose of comparison, frames from mechanized trials were compared with frames from control trials sampled at precise 5 s intervals.

Pressure and flow speed

Thermistor flow probes or pressure transducers were inserted into polyethylene cannulae (1.57 mm inner diameter, 2.08 mm outer diameter, Intramedic PE-205) passing through three 2.38 mm diameter holes in the model, two of them in the portion anterior to the first gill slot, and the third through the first branchial arch. The cannulae anterior to the first gill slots were oriented approximately perpendicular to the interior surface of the model, and were positioned opposite each other on either side of the anterior–posterior midline, and ventral to the model's lateral midline. The cannula through the first branchial arch was oriented so that the opening protruded through the posterior surface of the arch. Each cannula was flush with the interior surface of the model.

To measure flow speed, we used a probe constructed with a glass bead thermistor (1.09 mm diameter, 112-101BAJ-01, Fenwal Electronics) and connected to a circuit modified from LaBarbera and Vogel (1976). We measured pressure using a Millar Mikro-tip SPC-330 catheter pressure transducer (1.0 mm diameter) and a PCA-2 preamplifier and calibration unit. In previous studies (Patterson, 1991; Smith and Sanderson, 2008), this circuit with a glass bead thermistor of this size was described as having a frequency response of approximately 5 Hz, meaning events less than 200 ms in duration may not be detected consistently.

Pressure and flow speed were recorded from each cannula in four 90 s trials (one stationary control and three mechanized) at 200 Hz by a Sonometrics TRX-4A/D converter (Sonometrics Corporation, London, ON, Canada). To assess whether a higher frequency signal appearing in the readings was an artifact of the model mechanism, we also conducted a trial in which two 90 s recordings were taken from both anterior cannulae simultaneously.

Subsamples (75 s) of recordings were processed using a bandpass Fourier filter (1.8–2.6 Hz) in the ifilter: interactive Fourier filter function (version 4.1; O'Haver, 2014) add-on for MATLAB (version R2016a, 0.0.0.341360, MathWorks, Natick, MA, USA). We also used the ifilter function's power spectrum analysis tool to compare signal strength of various signal frequencies in mechanized and control trials.

To associate regions of pressure and velocity waveforms with particular portions of the model's stride, we conducted trials in which either flow speed or pressure was recorded at the model's left anterior cannula. Pressure and flow speed data were synchronized with video (Ektapro Hi-Spec motion analyzer 1012/2, 250 frames s^{-1}, Kodak, San Diego, CA), using a TTL-compatible trigger signal connected to the A/D converter. Peaks and troughs of pressure and flow speed were detected in seven-point moving averages of recorded pressure traces. When equivalent maximum or minimum pressure values occurred at multiple time points within a single stride, the earliest point with that value was used. We identified the times of the model's yaw maxima to either side in the videos, and calculated the mean delay between maximum yaw angles and recorded flow speed and pressure minima and maxima. The flow speed and pressure recordings made during these trials were used to calculate the differences between maximum and minimum recorded values in a stride.

Flow patterns

We used dye streams to visualize and qualitatively describe flow patterns through the model. Videos were recorded (240 frames s^{-1}) as rhodamine water-tracing dye (Cole-Parmer, Vernon Hills, IL, USA) was slowly introduced by syringe through the same polyethylene cannulae used for flow speed and pressure experiments. Digital particle image velocimetry was not feasible inside the model because the vortical flow structures formed medial to the mesh that simulated the gill rakers.

RESULTS
Particle transport

In experiments to quantify mesh coverage by particles during 3 min trials, stationary control trials exhibited significantly greater coverage of the portion of mesh analyzed than mechanized trials ($P<0.0005$), and there were also significant interactions for time and between treatment and time ($P<0.0005$ for both, two-way repeated-measures ANOVA, $n=4$ trials per group, 36 measurements per trial; Fig. 3). Only data from the final time point failed Levene's test for homogeneity of variances ($P=0.047$). After the completion of 3 min trials, models in control trials averaged 86.6±7.3% (95% CI) mesh coverage, while models in mechanized trials averaged 23.5±21.4% (95% CI) mesh coverage. In mechanized trials,
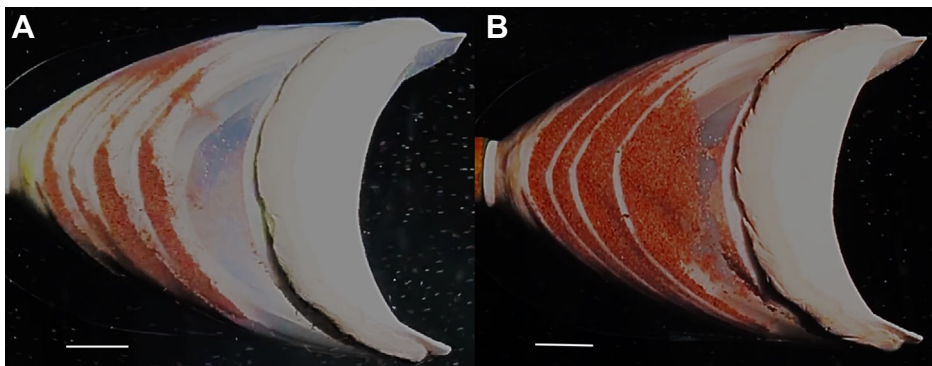
Fig. 4. Particle coverage of the mesh shown in lateral view after 3 min in a mechanized trial and a stationary control trial. (A) In mechanized trials, particles tended to collect in large aggregations in the posterior portions of the gill slots, especially in the ventral portion of the model. (B) In control trials, however, particles collected fairly evenly across much of the mesh. Scale bars, 1 cm. Model parameters for mechanized trials: 5 deg yaw, 1.1 cm heave, 72 deg yaw–heave phase difference, 2.2 Hz stride frequency.

particles were most often captured on the mesh along the posterior margins of each gill slot. By contrast, captured particles were more evenly distributed across the mesh in control trials (Fig. 4).

Pressure and flow speed

In all pressure and flow speed experiments, mechanized trials exhibited cyclical fluctuations at a frequency of 2.2 Hz, corresponding with the frequency of the model's strides (Fig. 5). In stationary control trials, no regular fluctuations in pressure or flow speed were observed or detected in Fourier transform analyses. Signals processed using a bandpass Fourier filter with a 0.8 Hz range centered around 2.2 Hz (Fig. 6), and power spectrum analyses using 75 s segments of flow speed and pressure recordings (Fig. 7) revealed that mechanized trials experienced pronounced increases in the amplitude and power of the signal at 2.2 Hz, as expected.

Secondary peaks were also detected in pressure and flow speed mechanized trials. It remains unclear whether these secondary peaks are a consequence of vortical flow patterns, an artifact of the model mechanism or both. However, in mechanized tests of the model in which pressure was recorded simultaneously by probes inserted through both left and right anterior cannulae, secondary peaks were recorded in comparable locations of both waveforms. These results indicate that if the secondary peaks did result from artifacts, the artifacts occurred at comparable times in both portions of the model's stride (left and right).

Using the pressure and flow data that had been synchronized with videos of the mechanized model's yaw maxima, we were able to determine that, when pressure is recorded at the left anterior cannula, there is a mean lag of 0.08 s (s.d.=0.01 s) between the maximum yaw to the model's right and the minimum recorded pressure in each stride, and a lag of 0.08 s (s.d.=0.02 s) between the
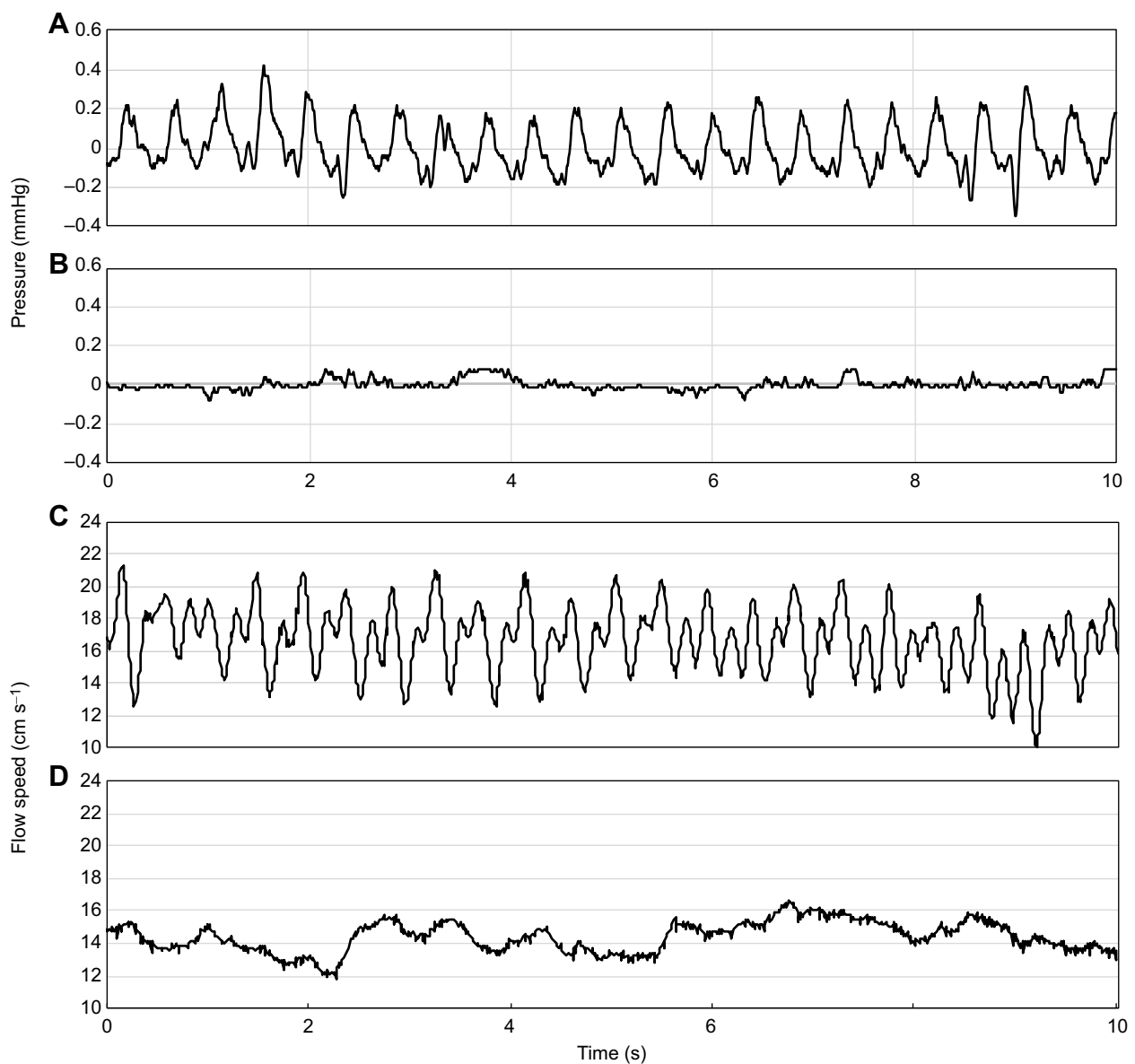
Fig. 5. Representative pressure and flow speed recordings from the left anterior cannula. (A,B) Pressure recordings in mechanized (A) and stationary control trials (B). Pressure values shown are seven-point moving averages of recorded data, and are presented as deviation from the mean value of each sample series. (C,D) Flow speed recordings in mechanized (C) and stationary control trials (D). Model parameters for mechanized trials: 5 deg yaw, 1.1 cm heave, 72 deg yaw–heave phase difference, 2.2 Hz stride frequency.
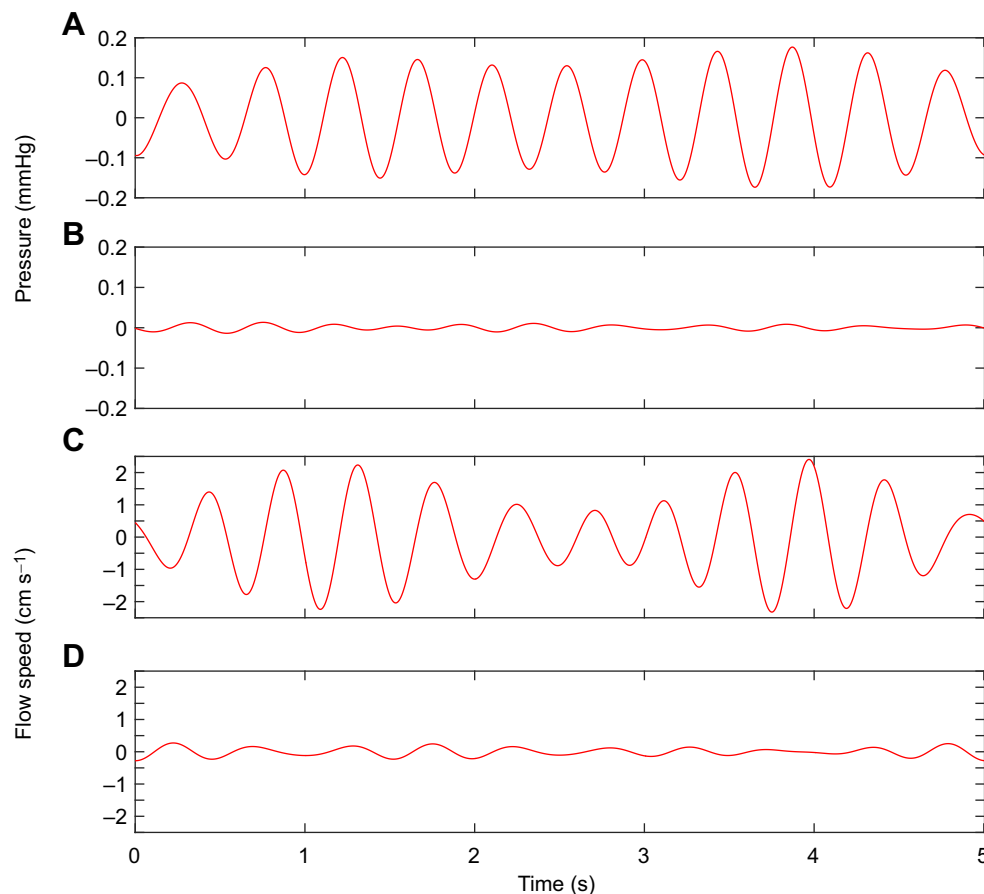
Fig. 6. Pressure and flow speed recordings filtered using a 1.8–2.6 Hz bandpass Fourier filter, which excluded all signals of frequencies outside that range. (A,B) Pressure recordings. (C,D) Flow speed recordings. Filtered signals from mechanized trials are shown in A and C, and signals from control trials are shown in B and D.

maximum yaw to the model's left and the maximum recorded pressure in each stride (data pooled from three series, each of n=44 strides for both calculations). At the same cannula, we measured a mean lag of 0.09 s (s.d.=0.05 s) between the maximum yaw to the model's right and the minimum recorded flow speed, and a mean lag of 0.13 s (s.d.=0.03 s) between the maximum yaw to the model's left and the maximum recorded flow speed (data pooled from three series, for first calculation n=43, 45 and 44 strides, for second calculation n=43, 44 and 44 strides).

In mechanized trials, the mean difference between minimum and maximum pressures recorded at the anterior cannula was 0.46 mmHg (s.d.=0.04 mmHg, data pooled from three series, N=392 total calculations, two per stride, n=113, 149, 130). The mean difference between minimum and maximum flow speeds was 5.26 cm s^{-1} (s.d.=1.14 cm s^{-1}, data pooled from three series, N=394 total calculations, two per stride, n=103, 191, 100). In one case, a stride was excluded from these calculations, because no peak in flow speed was detected in that stride, and thus the difference between the minimum and maximum values could not be calculated.

Flow patterns

In control trials, sustained vortical flow structures (Stel et al., 2012; Dol et al., 2014; Sanderson et al., 2016) were visible downstream of all cannulae through which dye was introduced. When dye was introduced through the cannulae positioned anterior to the first gill slot, a prominent vortical flow was visible along the anterior margin of the first gill slot (Fig. 8A). This vortical flow traveled continuously along the margin of the gill slot, primarily in a dorsal direction until dye dispersed. Most dye in this vortical flow

exited the model through the mesh near the posterior-most portion of the anterior margin of the first gill slot, just above the model's central coronal plane. This location approximately corresponds to the ceratobranchial–epibranchial joint in the paddlefish oral cavity. During control trials, the cannula inserted through the first branchial arch enabled visualization of smaller vortical flow structures along the anterior margin of the second gill slot (Fig. 8B). Dye introduced at this location exited the model directly through the mesh at the anterior margin of the second gill slot, with minimal travel along the posterior surface of the first branchial arch in either the dorsal or ventral direction.

In mechanized trials, vortical flow structures formed repeatedly because of flow separation in the anterior portion of the gill slot, and were then shed downstream. Entrained dye often traveled posteriorly after shedding, before exiting through the mesh (Fig. 9). These vortical structures tended to be shed as the model yawed to the side opposite the dye stream, although in some instances, they were shed only partially and rotation persisted throughout a stride. The vortical flow that formed along the anterior margin of the first gill slot was often accompanied by a second, separate vortical flow structure that formed anterior and dorsal to the opening of the cannula in the anterior portion of the model (Fig. 9B). This second flow structure rotated in the same direction as the first vortical flow described above, but formed less frequently, and was more disorganized and shorter-lived.

Vortical flow structures also briefly formed when dye was introduced through the cannula in the first branchial arch (Fig. 10). The speed at which the dye traveled in the time between exiting from the model's mesh in the second gill slot and leaving the simulated opercular cavity appeared to vary between portions of the model's
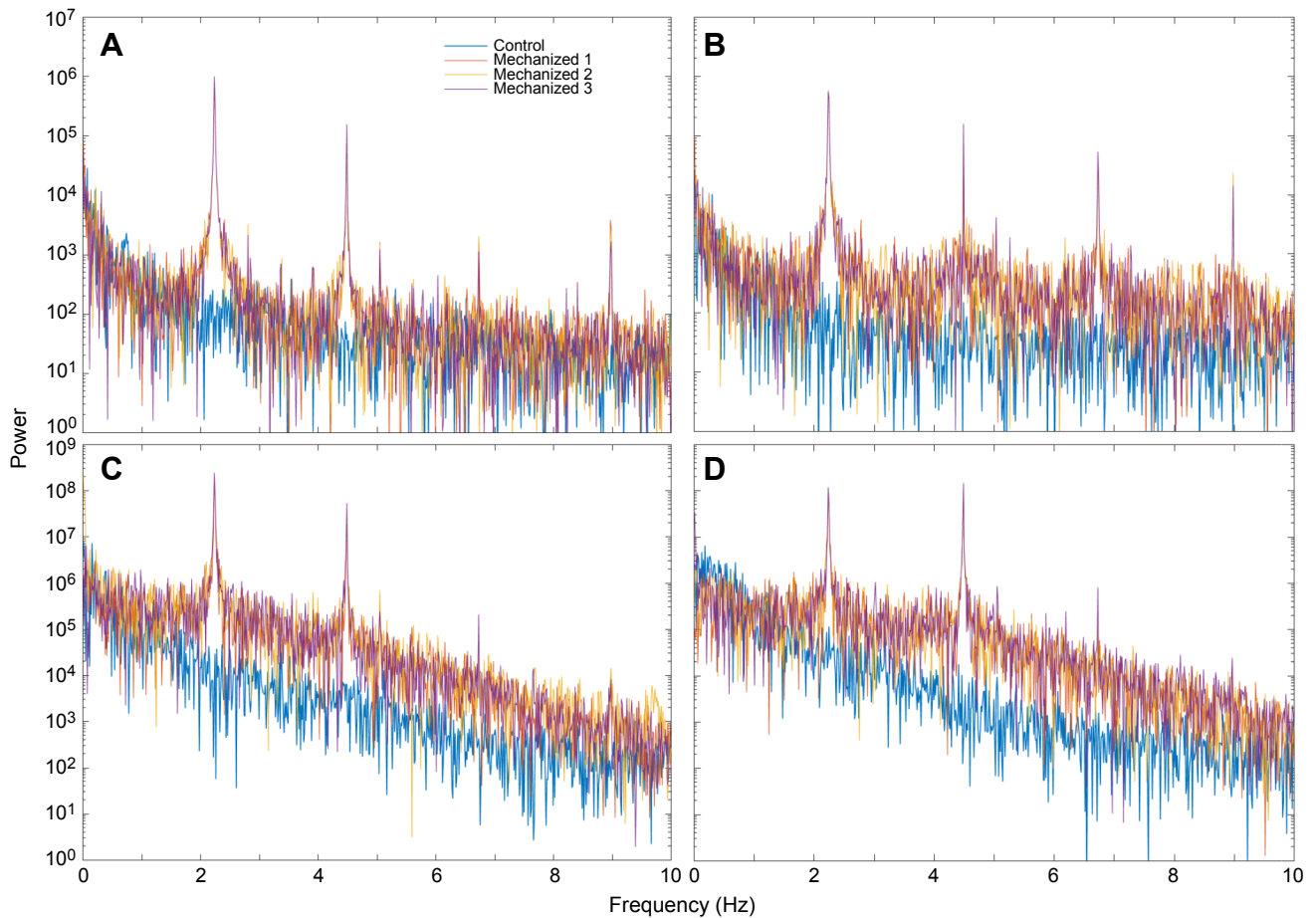
Fig. 7. Power spectrum comparisons of waveforms recorded during pressure and flow speed trials. (A,B) Data from pressure trials; (C,D) data from flow speed trials. The panels on the left show data recorded through the cannula in the branchial arch. The panels on the right show data recorded through the anterior cannula. All power analyses shown were computed using 75 s segments of recordings. Recordings from mechanized trials excluded at least the first two and final two strides of the model's operation in a trial.
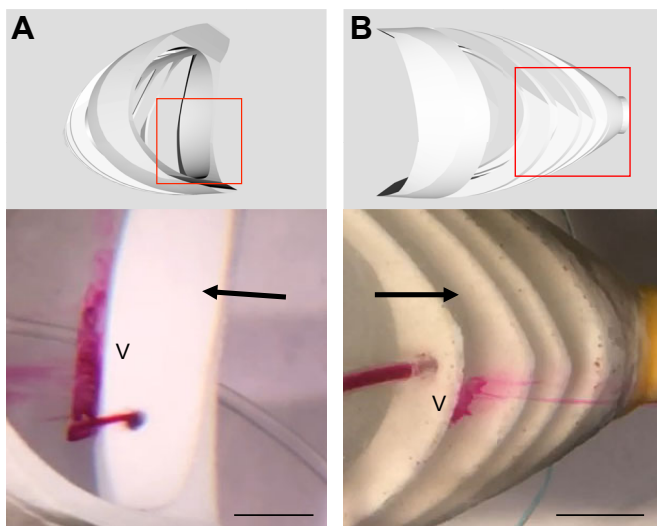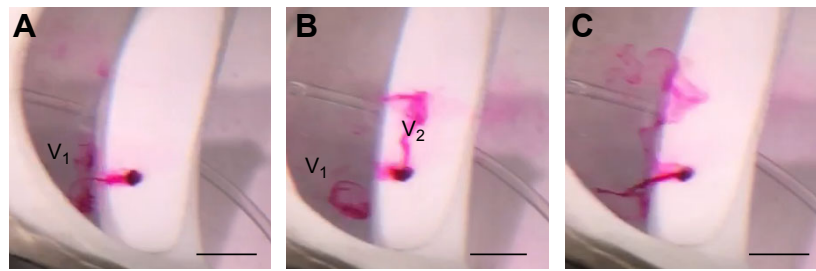

Fig. 8. Vortical flow structures (V) resulting from flow separation in stationary control models. (A) Dye release from the left anterior cannula, as viewed from the interior of the model. (B) Dye release from the left posterior cannula in the first branchial arch, as viewed from the exterior of the model. Red boxes indicate the portion of the model shown in the photographs. Scale bars, 1 cm. Arrows indicate direction of flow.

stride, indicating a change in the pressure gradient between the interior and exterior of the model. This dye stream appeared to move the fastest during and shortly following yaw peaks towards the same side of the model as dye introduction.

DISCUSSION

Effect of swimming kinematics on suspension feeding

We found that locomotor kinematics cause regular, cyclical fluctuations in flow speed and pressure in a model ram suspension-feeding paddlefish, as well as the formation and shedding of vortical flow structures downstream from the backward-facing steps formed by simulated branchial arches. These cyclical flow dynamics resulted in the transport of simulated food particles from the surface of the mesh simulating the gill rakers to aggregations of particles near the posterior margins of the gill slots. This reduced fouling of the filter, and moved particles to an area where they may be easier to manipulate and transport towards the esophagus. Reduction of filter fouling and increases in particle transport have been shown to result from bidirectional oscillatory flow and unidirectional pulsations in flow and transmembrane pressure in a variety of industrial and medical crossflow filtration systems (Jaffrin, 2012). Analogous flow manipulations have been quantified in pump suspension-feeding fish (Sanderson et al., 1991; Callan and Sanderson, 2003; Smith and Sanderson, 2008). Repetitive oscillatory and pulsatile flow patterns
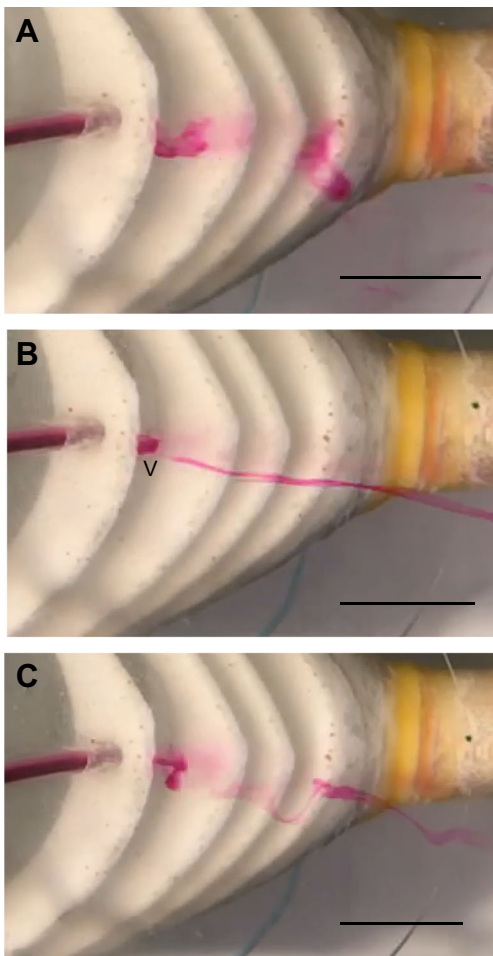
Fig. 9. Dye stream visualization of flow in the first gill slot on the left side of the mechanized model, as viewed from the interior of the model. In frame A, a vortical flow structure resulting from flow separation (V_1) is visible on the interior of the mesh, directly downstream from the backward-facing step formed at the anterior margin of the first gill slot. In frame B, the first vortical flow (V_1) has begun to decay, and a second (V_2) has formed anterior to the step. In frame C, both vortical flow structures are shed, and dye streams disperse downstream, tending to travel towards the posterior of the model before exiting through the mesh. Frame A occurs 0.225 s before frame B, which precedes frame C by 0.104 s. Frame A precedes the maximum yaw angle to the model's left by 0.096 s. Scale bars, 1 cm.

quantified in pump suspension-feeding fish have been suggested as de-fouling processes (Callan and Sanderson, 2003; Smith and Sanderson, 2008).

Previous investigations of the biomechanics of ram suspension-feeding fishes have used preserved specimens (Sanderson et al., 2016), physical models (Paig-Tran et al., 2011; Sanderson et al.,

Fig. 10. Dye stream visualization of flow in the second gill slot on the left side of the model in a mechanized trial, as viewed from the exterior of the model. A vortical flow structure (V) is shown in frame B, and shed through the mesh in frame C. Frame A occurred 0.067 s before the maximum yaw to the model's left, and preceded frame B by 0.163 s. Frame B preceded frame C by 0.108 s, which occurred 0.021 s before the model's maximum yaw to the right. Scale bars, 1 cm.

2016) and computational models (Cheer et al., 2012, 2001) to study the flow of water and food particles through the oral cavity and their interactions with gill rakers and branchial arches. However, while these studies have considered flow speed as a variable that is relevant to food particle size selectivity and the interactions between flow patterns and gill rakers, none have considered other kinematic variables associated with the undulatory locomotion used by most fish (Webb, 1975) as they relate to ram feeding. Sanderson et al. (1994), in the only known flow speed recordings taken from the interior of the oral cavity of live, ram suspension-feeding fish, showed that the flow speed measured during paddlefish suspension feeding (22–29 cm EFL) fluctuated at regular time intervals, though the cause of these fluctuations was not investigated at the time. Also, Burggren and Bemis (1992) recorded buccal pressure in a paddlefish (13.0 cm fork length) during ram ventilation and ventilation by buccal pumping, noting that pressure oscillations during ram ventilation reflected tailbeats.

Our findings indicate that in addition to the spatial organization of particle retention described in the vortical cross-step filtration mechanism of Sanderson et al. (2016), there also exists a strong temporal component to the organization of filtration mechanisms and particle retention patterns in ram suspension-feeding fish. The fluid dynamics of our model appear analogous to the unstable vortices resulting from pulsatile flow over a fixed backward-facing step (Dol et al., 2014), albeit with changes in the directionality of flow relative to anatomical structures as a consequence of yawing. A temporospatial cross-step filtration model that includes a kinematic mechanism for aggregating food particles at the posterior portion of the gill slot is applicable in both the paddlefish and the basking shark, two species that have convergently evolved rib-and-groove arrangements of their branchial arches. In these species, the gill rakers abduct from the distal regions of the branchial arches to form the porous floor of a groove that is roughly rectangular in cross-section (Imms, 1904; Matthews and Parker, 1950; Sanderson et al., 2016; Sims, 2008). This temporal organization of the cross-step model also clarifies the function of the mucus-secreting cells present on the branchial arch epithelium along the bases of the gill rakers in both the paddlefish and the basking shark. These mucus-secreting cells were previously presumed to be related to feeding, but, as the rakers themselves do not have mucus, were apparently of limited utility (Paig-Tran and Summers, 2014; Rosen and Hales, 1981; Matthews and Parker, 1950; Sims, 2008). Because our study demonstrates that fluid dynamics result in the transport of particles to the posterior margins of the gill slots, the mucus secretions of the branchial arch may function to form aggregations of food particles and mucus into a bolus or string that can be easily manipulated.

Journal of Experimental Biology

Our study has demonstrated that swimming kinematics aided the transport of simulated food to the posterior margins of the gill slots. Particles covered a significantly greater proportion of the mesh in models from stationary control trials compared with mechanized trials ($P<0.0005$). Within approximately 30 s, the proportion of the mesh covered by particles in the mechanized trials diverged from that of control trials (Fig. 3). The exact time to clogging in the models and in live ram suspension-feeding fish is expected to be strongly affected by the type, shape, size and concentration of prey that are encountered relative to the dimensions of the mesh and the gill raker filtration surfaces (Sanderson and Wassersug, 1993). Manipulation of these prey variables was beyond the scope of the present study, and our flow tank experiments focused on brine shrimp cysts of a specific shape, size and concentration. Future experiments could quantify the effects of different prey and prey concentrations on time to clogging in 3D models and on feeding bout duration in live ram suspension-feeding fish. Burggren and Bemis (1992) reported that paddlefish ram suspension feeding occurred 'in bursts of variable duration', and feeding bouts ranging from approximately 5 to 45 s have been observed (S.L.S., personal observation). In the videos that we used to quantify the swimming kinematics of paddlefish, the longest recorded uninterrupted bout of ram suspension feeding on adult brine shrimp, rather than brine shrimp cysts as we used in our flow tank experiments, was approximately 10 s. Because of the small size of the circular tanks used in our study, feeding bouts were often interrupted prematurely when fish collided with each other or the edge of the tank, or when they turned abruptly to evade collisions. While no data regarding duration of ram suspension-feeding bouts for paddlefish under natural conditions have been published, uninterrupted ram suspension-feeding bouts of 30–60 s (mean unreported) and bouts of 3.25–13 min (mean±s.e.m. 7.4±1.6 min, n=5) between 'coughs' to clear filter structures have been recorded for basking sharks (Sims, 2000b) and whale sharks (Motta et al., 2010), respectively, two species for which our findings may be applicable.

Although our experiments were conducted using a physical model of a rib-and-groove branchial arch structure, our results may also be applicable to teleost fishes using more typical crossflow filtration mechanisms (Sanderson et al., 2001). The ram suspension-feeding mechanisms in teleosts are not well studied compared with pump suspension feeding in teleost fishes that rely on suction, but the arrangement of the gill rakers on the branchial arches tends to be very different from the rib-and-groove arrangement of paddlefish and basking sharks. Instead of having gill rakers that protrude from the distal regions of the branchial arches, the gill rakers of ram suspension-feeding teleosts are attached to the medial edges of the arches (Sanderson et al., 1996, 2016). However, in the pump suspension-feeding blackfish (*Orthodon microlepidotus*, Cyprinidae; Sanderson et al., 1991) and blue tilapia (*Oreochromis aureus*, Cichlidae; Smith and Sanderson, 2008), regular fluctuations in flow speed have been recorded that were similar to those we measured in our physical model as well as those that Sanderson et al. (1994) measured in live paddlefish. Furthermore, the influence of crossflow is strong enough in pump suspension-feeding cichlids that fish may feed effectively even when gill rakers are surgically removed (Smith and Sanderson, 2007, 2013; Drenner et al., 1987). Transport of food particles may be facilitated in an analogous manner in teleost ram suspension feeders by kinematically modulated hydrodynamic processes that influence pressure gradients and flow patterns, which in turn minimize particle contact with gill rakers or resuspend captured particles from the filter apparatus.

In addition to aiding in the manipulation of food towards the esophagus, the clearing of food particles from the surface of the filter apparatus during ram suspension feeding is likely to allow more efficient respiration by permitting a larger volume of water to flow through the gill slots than would otherwise be possible. This would at least partially resolve the functional conflict between respiration and suspension feeding that Feder et al. (1984) demonstrated in *Xenopus* larvae, and Sanderson et al. (1994) predicted to exist in fish, in which maximizing prey capture reduces the effectiveness of respiratory structures. Burggren and Bemis (1992) suggested that ram suspension feeding permits more efficient use of energy in ram ventilators, and that the evolution of suspension feeding in the *Polyodon* genus (Grande and Bemis, 1991) was made more likely by the 'preadaptation' of ram ventilation because simultaneous ram feeding and ventilation reduces the metabolic costs of both foraging and opercular pumping. This view would be further supported by showing that clearing of gill rakers by flow dynamics associated with swimming kinematics increases respiratory efficiency compared with rakers clogged with food particles.

Ecological implications
Because swimming during ram suspension feeding is much more metabolically expensive than routine swimming as a result of the increased drag that results from swimming with a large open gape (James and Probyn, 1989; Durbin et al., 1981), ram suspension feeders require certain threshold densities of zooplankton to feed at a net energy gain (Sims, 1999, 2000a). These prey threshold densities are measurable in several different ways, yielding relatively consistent results in mass of prey per volume of water (Sims, 1999). However, Sims (2000b) also noted that basking sharks swim more slowly during suspension feeding than the speeds at which they had been predicted to maximize net energy gain based on evidence from teleost ram suspension feeders. This was partially attributed to the increased effect of skin friction drag in basking sharks (Sims, 2000a), but could also be partly explained by increased functionality of the filter apparatus, at least for small particles, at lower speeds. Using a computational fluid dynamics (CFD) model, Cheer et al. (2012) demonstrated that the gill rakers of ram suspension feeders are less leaky at low Reynolds numbers. Because intra-oral flow speeds, as well as pressure and the incident angle of flow, are constantly changing in association with swimming kinematics, it is possible that these variables affect the size selectivity of particles smaller than the inter-raker space.

Rubenstein and Koehl (1977) have previously hypothesized that, as a way to increase particle capture using filtration mechanisms, filter-feeding organisms might move more quickly than when cruising. Pepin et al. (1988) provided strong empirical evidence that this is the case in ram suspension-feeding Atlantic mackerel (*Scomber scombrus*). However, this was proposed in the context of filter fibers capturing particles by inertial impaction, with retention often facilitated by mucus, or sieving (Shimeta and Jumars, 1991). In the context of crossflow filtration, in which fish retain food particles primarily by inertial lift and shear-induced diffusion as water passes across, rather than through, a filter apparatus (Sanderson et al., 2001; van Dinther et al., 2011), there could be combinations of slower flow speeds, and particle sizes and densities, that might allow the capture of more, rather than fewer, particles smaller than the inter-raker gaps. Furthermore, although the inter-raker distances are unavailable for *S. scombrus*, if the relationship between body length and inter-raker distance is similar to that observed in the congeneric Pacific mackerel (*S. japonicus*;

Molina et al., 1996), then all size classes of plankton used by Pepin et al. (1988) would have been larger than the inter-raker space, and thus easily retained by the fish irrespective of swimming speed.

Paig-Tran et al. (2011) found that retention of particles smaller than their model's mesh pore diameter improved at higher flow speeds (60 cm s^{-1} compared with 45 cm s^{-1}). However, they compared capture on the filter mesh in their models, and in a fish employing crossflow filtration, particles smaller than the inter-raker space would not tend to be captured on the surface of the rakers. In addition, Paig-Tran et al. (2011) only measured particles captured at their model's simulated esophagus from 45 cm s^{-1} trials. Particle separation has also been shown in a biomimetic crossflow filter design to decline at increasing, but biologically relevant flow speeds (Hung et al., 2012). Therefore, because it is now clear that swimming kinematics including yaw and heave result in changes in intra-oral flow speeds and patterns, it is conceivable that fish adjust swimming kinematics in order to modulate mechanical size selectivity of the filter apparatus and increase the amount of prey captured, especially when available zooplankton are smaller than the inter-raker distance. This hypothesis could be tested in laboratory experiments by quantifying the swimming speeds and kinematics of ram suspension-feeding fish in aquaria seeded with zooplankton prey of sizes larger than the fishes' inter-raker space, and comparing these with the speeds and kinematics of fish ram suspension feeding in aquaria seeded with zooplankton prey of sizes smaller than the fishes' inter-raker space.

Determining in as much detail as possible how ram suspension feeders are able to filter prey from the water column is of substantial interest, as many of these species are of economic importance (Food and Agriculture Organization of the United Nations, 2016) and serve as ecologically important links between phytoplankton or zooplankton and larger piscivorous predators. As a consequence, the ability to develop more accurate predictive models of population growth and decline would be of value to both commercial fisheries and conservation efforts. For example, Annis et al. (2011) specifically report that more information regarding size selectivity in Atlantic menhaden would be likely to produce population and growth models more capable of responding to trends in plankton communities. However, without a better understanding of the mechanics of suspension feeding, this remains difficult, especially because of the complex nature of prey selection. Researchers have shown, for instance, that texture in addition to size is important in determining the ability of a fish to capture certain prey items (Garrido et al., 2007), that suspension-feeding fish prey on the eggs and larvae of other fish (Garrido et al., 2007; Molina et al., 1996), and that in some closely related species, including the menhaden *Brevoortia gunteri* and *B. patronus*, seasonal partitioning of food resources takes place on the basis of prey size, despite similar gill raker structures (Castillo-Rivera et al., 1996).

Future directions
Our experiments have shown that there is strong integration between feeding and swimming kinematics in ram suspension-feeding fish. However, to build a more complete understanding of how ram suspension-feeding fish respond to and influence aquatic and marine communities, experimental studies using model ram suspension-feeding teleosts will be needed to show the impact of swimming kinematics on feeding in species without the rib-and-groove branchial arch structure of paddlefish and basking sharks. Ideally, these studies should incorporate investigations of various kinematic parameters including swimming speed, yaw angles, phase difference between yaw and heave, and stride frequency.

Similar physical model-based, CFD or live-animal studies of kinematic influence on feeding in the whale shark, megamouth shark and mobulid rays, all of which have filtration structures that are highly divergent from those in the paddlefish and basking shark (Paig-Tran and Summers, 2014), should also be pursued. Finally, CFD studies that investigate how locomotor kinematics influence size selectivity of filter structures, especially for very small particles, would establish a strong link between the functional morphology and biomechanics of ram suspension-feeding fishes and the ecological implications of this feeding mode.

References
Akanyeti, O., Thornycroft, P. J. M., Lauder, G. V., Yanagitsuru, Y. R., Peterson, A. N. and Liao, J. C. (2016). Fish optimize sensing and respiration during undulatory swimming. *Nat. Commun.* **7**, 11044.

Annis, E. R., Houde, E. D., Harding, L. W., Jr, Mallonee, M. E. and Wilberg, M. J. (2011). Calibration of a bioenergetics model linking primary production to Atlantic menhaden *Brevoortia tyrannus* growth in Chesapeake Bay. *Mar. Ecol. Prog. Ser.* **437**, 253-267.

Bainbridge, R. (1958). The speed of swimming fish as related to size and to the frequency and amplitude of the tail beat. *J. Exp. Biol.* **35**, 109-133.

Bainbridge, R. (1963). Caudal fin and body movement in the propulsion of some fish. *J. Exp. Biol.* **40**, 23-56.

Brainerd, E. L. (2001). Caught in the crossflow. *Nature* **412**, 387-388.

Burggren, W. W. and Bemis, W. E. (1992). Metabolism and ram gill ventilation in juvenile paddlefish, *Polyodon spathula* (Chondrostei: Polyodontidae). *Physiol. Zool.* **65**, 515-539.

Callan, W. T. and Sanderson, S. L. (2003). Feeding mechanisms in carp: crossflow filtration, palatal protrusions and flow reversals. *J. Exp. Biol.* **206**, 883-892.

Castillo-Rivera, M., Kobelkowski, A. and Zamayoa, V. (1996). Food resource partitioning and trophic morphology of *Brevoortia gunteri* and *B. patronus*. *J. Fish Biol.* **49**, 1102-1111.

Cheer, A. Y., Ogami, Y. and Sanderson, S. L. (2001). Computational fluid dynamics in the oral cavity of ram suspension-feeding fishes. *J. Theor. Biol.* **210**, 463-474.

Cheer, A., Cheung, S., Hung, T.-C., Piedrahita, R. H. and Sanderson, S. L. (2012). Computational fluid dynamics of fish gill rakers during crossflow filtration. *Bull. Math. Biol.* **74**, 981-1000.

Dewar, H. and Graham, J. B. (1994). Studies of tropical tuna swimming performance in a large water tunnel. *J. Exp. Biol.* **192**, 45-59.

Dol, S. S., Salek, M. M. and Martinuzzi, R. J. (2014). Effects of pulsation to the mean field and vortex development in a backward-facing step flow. *J. Fluids Eng.* **136**, 011001.

Drenner, R. W., Hambright, K. D., Vinyard, G. L. and Gophen, M. (1987). Particle ingestion by *Tilapia galilaea* is not affected by removal of gill rakers and microbranchiospines. *Trans. Am. Fish. Soc.* **116**, 272-276.

Durbin, A. G., Durbin, E. G., Verity, P. G. and Smayda, T. J. (1981). Voluntary swimming speeds and respiration rates of a filter-feeding planktivore, the Atlantic menhaden, *Brevoortia tyrannus* (Pisces: Clupeidae). *Fish. Bull.* **78**, 877-886.

Feder, M. E., Seale, D. B., Boraas, M. E., Wassersug, R. J. and Gibbs, A. G. (1984). Functional conflicts between feeding and gas exchange in suspension-feeding tadpoles, *Xenopus lævis*. *J. Exp. Biol.* **110**, 91-98.

Ferry, L. A., Paig-Tran, E. M. and Gibb, A. C. (2015). Suction, ram, and biting: deviations and limitations to the capture of aquatic prey. *Integr. Comp. Biol.* **55**, 97-109.

Food and Agriculture Organization of the United Nations. (2016). *Fishery and Aquaculture Statistics, Capture and Production by Principal Species in 2014.* Rome: FAO.

Friedland, K. D., Ahrenholz, D. W., Smith, J. W., Manning, M. and Ryan, J. (2006). Sieving functional morphology of the gill raker feeding apparatus of Atlantic menhaden. *J. Exp. Zool.* **305A**, 974-985.

Garrido, S., Marçalo, A., Zwolinski, J. and van der Lingen, C. D. (2007). Laboratory investigations on the effect of prey size and concentration on the feeding behaviour of *Sardina pilchardus. Mar. Ecol. Prog. Ser.* **330**, 189-199.

Grande, L. and Bemis, W. E. (1991). Osteology and phylogenetic relationships of fossil and recent paddlefishes (Polyodontidae) with comments on the interrelationships of Acipenseriformes. *J. Verteb. Paleontol. Memoir 1* **11**, 1-121.

Higham, T. E., Rogers, S. M., Langerhans, R. B., Jamniczky, H. A., Lauder, G. V., Stewart, W. J., Martin, C. H. and Reznick, D. N. (2016). Speciation through the lens of biomechanics: locomotion, prey capture and reproductive isolation. *Proc. R. Soc. B* **283**, 20161294.

Hoogenboezem, W. (2000). On the feeding biology of bream (*Abramis brama*). *Neth. J. Zool.* **50**, 225-232.

Hoogenboezem, W., Lammens, E. H. R. R., MacGillavry, P. J. and Sibbing, F. A. (1993). Prey retention and sieve adjustment in filter-feeding bream (*Abramis brama*) (Cyprinidae). *Can. J. Fish. Aquat. Sci.* **50**, 465-471.

Hung, T.-C., Piedrahita, R. H. and Cheer, A. (2012). Bio-inspired particle separator design based on the food retention mechanism by suspension-feeding fish. *Bioinspir. Biomim.* **7**, 046003.

Imms, A. D. (1904). Notes on the gill-rakers of the spoonbill sturgeon, *Polyodon spathula. Proc. Zool. Soc. Lond.* **2**, 22-35.

Jaffrin, M. Y. (2012). Hydrodynamic techniques to enhance membrane filtration. *Annu. Rev. Fluid Mech.* **44**, 77-96.

James, A. G. and Probyn, T. (1989). The relationship between respiration rate, swimming speed and feeding behaviour in the Cape anchovy *Engraulis capensis* Gilchris. *J. Exp. Mar. Biol. Ecol.* **131**, 81-100.

Kane, E. A. and Higham, T. E. (2015). Complex systems are more than the sum of their parts: using integration to understand performance, biomechanics, and diversity. *Integr. Comp. Biol.* **55**, 146-165.

LaBarbera, M. (1984). Feeding currents and particle capture mechanisms in suspension feeding animals. *Am. Zool.* **24**, 71-84.

LaBarbera, M. and Vogel, S. (1976). Inexpensive thermistor flowmeter for aquatic biology. *Limnol. Oceanogr.* **21**, 750-756.

Lighthill, J. (1993). Estimates of pressure differences across the head of a swimming clupeid fish. *Philos. Trans. Biol. Sci.* **341**, 129-140.

Matthews, L. H. and Parker, H. W. (1950). Notes on the anatomy and biology of the basking shark (*Cetorhinus maximus* (Gunner)). *Proc. Zool. Soc. Lond.* **120**, 535-576.

Molina, R. E., Manrique, F. A. and Velasco, H. E. (1996). Filtering apparatus and feeding of the Pacific mackerel (*Scomber japonicus*) in the Gulf of California. *California Coop. Oceanic Fish. Invest. Rep.* **37**, 251-256.

Motta, P. J., Maslanka, M., Hueter, R. E., Davis, R. L., de la Parra, R., Mulvany, S. L., Habegger, M. L., Strother, J. A., Mara, K. R., Gardiner, J. M. et al. (2010). Feeding anatomy, filter-feeding rate, and diet of whale sharks *Rhincodon typus* during surface ram filter feeding off the Yucatan Peninsula, Mexico. *Zoology* **113**, 199-212.

Müller, U. K., Stamhuis, E. J. Videler, J. J. (2002). Riding the waves: the role of the body wave in undulatory fish swimming. *Integr. Comp. Biol.* **42**, 981-987.

Norton, S. F. and Brainerd, E. L. (1993). Convergence in the feeding mechanics of ecomorphologically similar species in the Centrarchidae and Cichlidae. *J. Exp. Biol.* **176**, 11-29.

O'Haver, T. C. (2014). ifilter: Interactive Fourier filter function, Version 4.1. https://terpconnect.umd.edu/~toh/spectrum/InteractiveFourierFilter.htm.

Paig-Tran, E. W. M. and Summers, A. P. (2014). Comparison of the structure and composition of the branchial filters in suspension feeding elasmobranchs. *Anat. Rec.* **297**, 701-715.

Paig-Tran, E. W. M., Bizzarro, J. J., Strother, J. A. and Summers, A. P. (2011). Bottles as models: predicting the effects of varying swimming speed and morphology on size selectivity and filtering efficiency in fishes. *J. Exp. Biol.* **214**, 1643-1654.

Patterson, M. R. (1991). The effects of flow on polyp-level prey capture in an octocoral, *Alcyonium siderium. Biol. Bull.* **180**, 93-102.

Pepin, P., Koslow, J. A. and Pearre, S.Jr. (1988). Laboratory study of foraging by Atlantic mackerel, *Scomber scombrus*, on natural zooplankton assemblages. *Can. J. Fish. Aquat. Sci.* **45**, 879-887.

Pyatetskiy, V. E. (1970a). Kinematic characteristics of some fast marine fish. *Bionika* **1970**, 11-20. In Webb 1975.

Pyatetskiy, V. E. (1970b). Hydrodynamic characteristics of swimming of some fast marine fish. *Bionika* **1970**, 20-27. In Webb 1975.

Rosen, R. A. and Hales, D. C. (1981). Feeding of paddlefish, *Polyodon spathula. Copeia* **1981**, 441-455.

Rowe, D. M., Denton, E. J. and Batty, R. S. (1993). Head turning in herring and some other fish. *Philos. Trans. Biol. Sci.* **341**, 141-148.

Rubenstein, D. I. and Koehl, M. A. R. (1977). The mechanisms of filter feeding: some theoretical considerations. *Am. Nat.* **111**, 981-994.

Sanderson, S. L. and Wassersug, R. (1993). Convergent and alternative designs for vertebrate suspension feeding. In *The Skull: Functional and Evolutionary Mechanisms* (ed. J. Hanken and D. K. Hall), pp. 37-112. Chicago, IL: The University of Chicago Press.

Sanderson, S. L., Cech, J. J. and Patterson, M. R. (1991). Fluid dynamics in suspension-feeding blackfish. *Science* **251**, 1346-1348.

Sanderson, S. L., Cech, J. J., Jr and Cheer, A. Y. (1994). Paddlefish buccal flow velocity during ram suspension feeding and ram ventilation. *J. Exp. Biol.* **186**, 145-156.

Sanderson, S. L., Chesnutt, C. R. and Lobel, P. S. (1996). Evidence for ram suspension feeding by the piscivore, *Seriola dumerili* (Carangidae). *Environ. Biol. Fishes* **46**, 365-373.

Sanderson, S. L., Cheer, A. Y., Goodrich, J. S., Graziano, J. D. and Callan, W. T. (2001). Crossflow filtration in suspension-feeding fishes. *Nature* **412**, 439-441.

Sanderson, S. L., Roberts, E., Lineburg, J. and Brooks, H. (2016). Fish mouths as engineering structures for vortical cross-step filtration. *Nat. Commun.* **7**, 11092.

Shelton, R. M., Thornycroft, P. J. M. and Lauder, G. V. (2014). Undulatory locomotion of flexible foils as biomimetic models for understanding fish propulsion. *J. Exp. Biol.* **217**, 2110-2120.

Shimeta, J. and Jumars, P. A. (1991). Physical mechanisms and rates of particle capture by suspension-feeders. *Oceanogr. Mar. Biol.* **29**, 191-257.

Sims, D. W. (1999). Threshold foraging behaviour of basking sharks on zooplankton: life on an energetic knife-edge? *Proc. R. Soc. B* **266**, 1437-1443.

Sims, D. W. (2000a). Can threshold foraging responses of basking sharks be used to estimate their metabolic rate? *Mar. Ecol. Prog. Ser.* **200**, 289-296.

Sims, D. W. (2000b). Filter-feeding and cruising swimming speeds of basking sharks compared with optimal models: they filter-feed slower than predicted for their size. *J. Exp. Mar. Biol. Ecol.* **249**, 65-76.

Sims, D. W. (2008). Sieving a living: a review of the biology, ecology and conservation status of the plankton-feeding basking shark *Cetorhinus maximus*. In *Advances in Marine Biology*, Vol. 54 (ed. D. W. Sims), pp. 171-220. Oxford, UK: Academic Press.

Smith, J. C. and Sanderson, S. L. (2007). Mucus function and crossflow filtration in a fish with gill rakers removed *versus* intact. *J. Exp. Biol.* **210**, 2706-2713.

Smith, J. C. and Sanderson, S. L. (2008). Intra-oral flow patterns and speeds in a suspension-feeding fish with gill rakers removed versus intact. *Biol. Bull.* **215**, 309-318.

Smith, J. C. and Sanderson, S. L. (2013). Particle retention in suspension-feeding fish after removal of filtration structures. *Zoology* **116**, 348-355.

Stel, H., Franco, A. T., Junqueira, S. L. M., Erthal, R. H., Mendes, R., Gonçalves, M. A. L. and Morales, R. E. M. (2012). Turbulent flow in d-type corrugated pipes: flow pattern and friction factor. *J. Fluid. Eng.* **134**, 121202.

Tanaka, H., Aoki, I. and Ohshimo, S. (2006). Feeding habits and gill raker morphology of three planktivorous pelagic fish species off the coast of northern and western Kyushu in summer. *J. Fish Biol.* **68**, 1041-1061.

Tytell, E. D., Borazjani, I., Sotiropoulos, F., Baker, T. V., Anderson, E. J. and Lauder, G. V. (2010). Disentangling the functional roles of morphology and motion in the swimming of fish. *Integr. Comp. Biol.* **50**, 1140-1154.

van Dinther, A. M. C., Schroën, C. G. P. H. and Boom, R. M. (2011). High-flux membrane separation using fluid skimming dominated convective fluid flow. *J. Membr. Sci.* **371**, 20-27.

Webb, P. W. (1971). The swimming energetics of trout, 1. Thrust and power output at cruising speeds. *J. Exp. Biol.* **55**, 489-520.

Webb, P. W. (1975). Hydrodynamics and energetics of fish propulsion. *Bull. Fish. Res. Board Canada* **190**, 1-159.

Webb, P. W. (1986). Kinematics of lake sturgeon, *Acipenser fulvescens*, at cruising speeds. *Can. J. Zool.* **64**, 2137-2141.

Webb, P. W. (1988). 'Steady' swimming kinematics of tiger musky, an esociform accelerator, and rainbow trout, a generalist cruiser. *J. Exp. Biol.* **138**, 51-69.

Webb, P. W. (1992). Is the high cost of body/caudal fin undulatory swimming due to increased friction drag or inertial recoil? *J. Exp. Biol.* **162**, 157-166.

Webb, P. W., Kostecki, P. T. and Stevens, E. D. (1984). The effect of size and swimming speed on locomotor kinematics of rainbow trout. *J. Exp. Biol.* **109**, 77-95.

Weihs, D. (2002). Stability versus maneuverability in aquatic locomotion. *Integr. Comp. Biol.* **42**, 127-134.

Zamon, J. E. (2003). Mixed species aggregations feeding upon herring and sandlance schools in a nearshore archipelago depend on flooding tidal currents. *Mar. Ecol. Prog. Ser.* **261**, 243-255.